Supporting Information

for

Facile citrate gel synthesis of antimony-carbon nanosponge with enhanced lithium storage

Hang T. T. Le[a,#], *Xuan-Manh Pham*[b,#] *and Chan-Jin Park*[b,*]

[#] These authors contributed equally to this study

[a] School of Chemical Engineering, Hanoi University of Science and Technology, 1 Dai Co Viet, Hai Ba Trung, Hanoi, Vietnam

[b] Department of Materials Science and Engineering, Chonnam National University, 77, Yongbongro, Bukgu, Gwangju 500-757, South Korea

* Corresponding author

E-mail: parkcj@jnu.ac.kr

Fax: +82-62-530-1699

Tel: +82-62-530-1704

Table S1. Elemental composition of Sb@C nanocomposite samples

Sample	Weight content [wt%]					
	N	C	H	S	O	Sb
Sb@C -1	0	26.87	1.52	0	0.75	70.86
Sb@C-2	0	39.22	1.78	0	1.14	57.86
Sb@C-3	0	44.65	1.68	0	2.78	50.89
Sb@C-4	0	49.93	1.57	0	2.79	45.71

The weight content of nitrogen, carbon, hydrogen, and sulfur elements present in the Sb@C composite samples were determined by elemental analysis (CHNS-O). The remaining weight percentage is assigned to Sb. The presence of oxygen in the composite is attributed to the adsorption of oxygen in the air atmosphere on the surface of the synthesized composite. As shown in **Table S1**, oxygen content increases with the increase of carbon content. This implies that a more porous structure with a high specific surface area was formed as the carbon precursor content increased.

Table S2 - Fitting parameters obtained from the impedance spectra for the as-prepared Sb electrode, as-prepared Sb@C-3 electrode and Sb@C-3 electrode after the charge-discharge test for 500 cycles at the 1C-rate.

Sample	R_e	R_{int}	CPE_{int}		R_{ct}	CPE_{ct}		W
	(Ω)	**(Ω)**	C_{int} **(F)**	n_{int}	**(Ω)**	C_{ct} **(F)**	n_{ct}	**(Ω^{-1} $s^{1/2}$)**
As-prepared Sb	8.1	-	-	-	198.2	1.99×10^{-6}	0.740	1.85×10^{-4}
As-prepared Sb@C-3	7.8	-	-	-	109.9	2.79×10^{-6}	0.754	3.29×10^{-4}
Sb@C-3 after 500 cycles	7.9	271.5	1.42×10^{-6}	0.757	98.6	52.92×10^{-6}	0.782	0.32×10^{-4}

Table S3 - Comparison of electrochemical performance of Sb/C composite anodes for lithium-ion batteries

Anode	Cycling stability	Rate capability	Synthesis methods	Ref.
Sb@C nanosponge	447.1 mAh g^{-1} after 500 cycles at 1 C (0.66 A g^{-1})	405.97 mAh g^{-1} at 10 C (6.6 A g^{-1})	Citrate gel synthesis	This work
Sb–graphite	550 mAh g^{-1} after 250 cycles at 230 mA g^{-1}	317 mA h g^{-1} at 4C (2.3 A g^{-1})	Ball milling	[1]
Sb/C composite	466.2 mAh g^{-1} after 200 cycle at 100 mA g^{-1}	354.4 mAh g^{-1} at 1 A g^{-1}	Sol–gel routine	[2]
Spherical Sb/C	590 mAh g^{-1} after 80 cycles at 100 mA g^{-1}.	535 mAh g^{-1} at 1.2 A g^{-1}	Aerosol spray pyrolysis technique	[3]
Rod-like Sb/C	478.8 mAh g^{-1} after 100 cycles at 100 mA g^{-1}	369.7 mAh g^{-1} at 0.5 A g^{-1}	Reduction and carbon deposition	[4]
Sb@C/expanded graphite	486 mAh g^{-1} after 600 cycles at 1 A g^{-1}	287 mAh g^{-1} at 2 A g-1	Freeze dying	[5]
Sb/C polyhedra	400.5 mAh g^{-1} after 500 cycles at 1 A g^{-1}	437.1 mAh g^{-1} at 5 A g^{-1}	Galvanic replacement	[6]
Sb/C fiber	254.4 mAh g^{-1} after 100 cycles at 100 mA g^{-1}	149.8 mAh g^{-1} at 1.6 A g^{-1}	Electrospinning	[7]
Sb/CNT composite	277.2 mA h g^{-1} after 50 cycles at 25 mA g^{-1}	-	Ball milling	[8]
Rod-like Sb/NPC	556 mA h g^{-1} after 100 cycles at 200 mA g^{-1}	312.3 mAh g^{-1} at 5 A g^{-1}	In-situ nanoconfined replacement reaction	[9]
Hollow Sb@C	405 mA h g^{-1} after 300 cycles at 1 A g^{-1}	384 mAh g^{-1} at 2 A g^{-1}	Nanoconfined galvanic replacement route	[10]

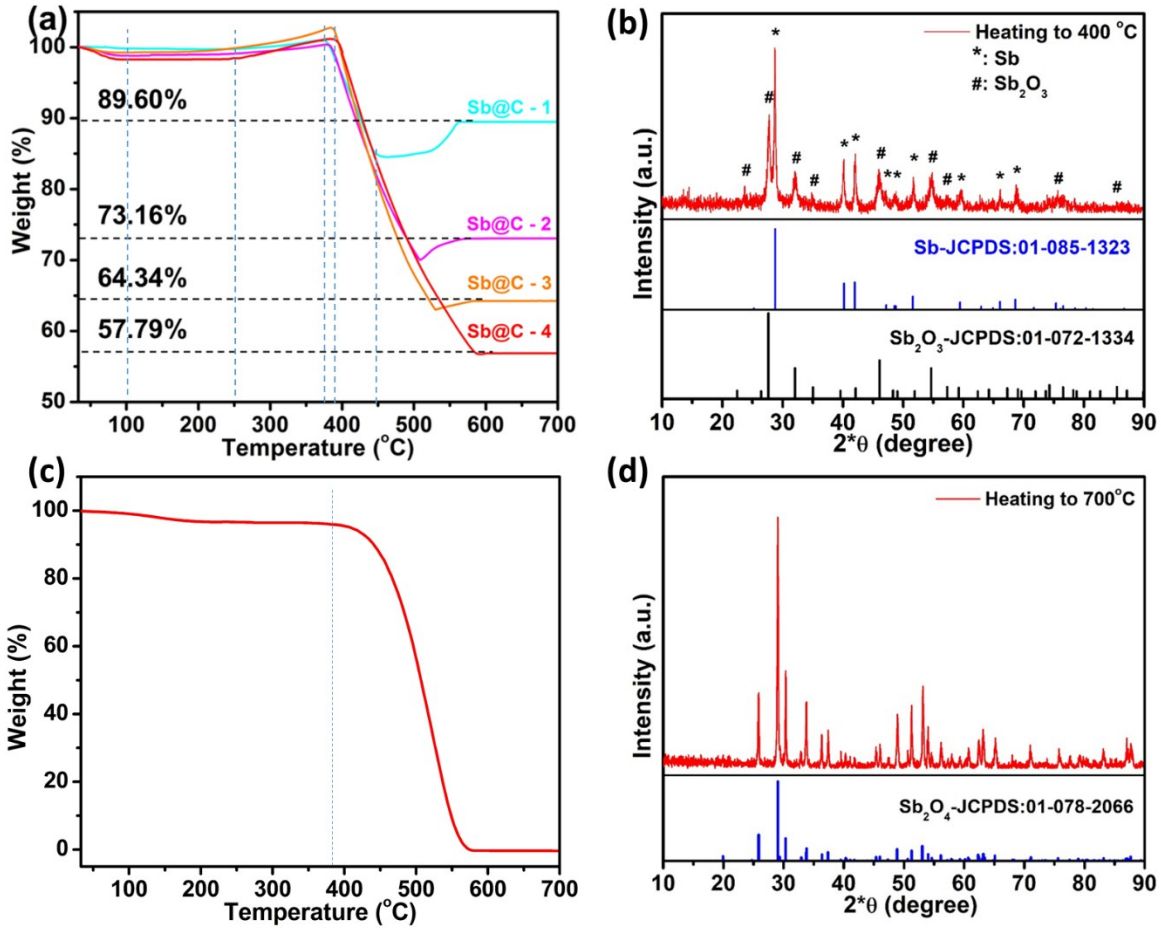

Fig. S1*: (a) TGA curves of Sb@C samples in air; (b) Thermogravimetric (TG) plot of pyrolytic carbon sample synthesized by carbonizing citric acid under the same conditions with the Sb@C samples. XRD patterns of Sb@C composite samples after heating at (c) 400 ºC and (d) 700 ºC in air.*

Fig. S1a shows TGA curves of the Sb@C composites. It is recognized that all Sb@C samples exhibit the similar TGA behavior. In specific, the samples revealed the first weight loss near 100 ºC, which originates from the removal of moisture from the samples. Subsequently, the weight of the samples almost remained until the temperature reached 250 ºC. After that, when the temperature continuously increased, the samples showed a slight increase in weight as a consequence of partial oxidation of metallic Sb to Sb_2O_3 (**Fig. S1**b), according to the following reaction:

$$4Sb + 3O_2 \rightarrow 2Sb_2O_3 \qquad (S1)$$

After reaching the temperature of near 400 ºC, the Sb@C samples exhibited significant weight loss, which was attributed to carbon combustion (**Fig. S1**a):

$$C + O_2 \rightarrow CO_2 \qquad (S2)$$

The similar phenomenon of combustion reaction was found for the pyrolytic carbon sample synthesized by carbonizing citric acid under the same conditions with the Sb@C samples (**Fig. S1**c).

The last weight change of the Sb@C composites is observed at the temperature from ~ 450 ºC to 600 ºC, which corresponds to the further oxidation of Sb_2O_3 as well as the residual Sb by forming other oxides of Sb, e.g., Sb_2O_4 (**Fig. S1**d):

$$2Sb_2O_3 + O_2 \rightarrow 2Sb_2O_4 \qquad (S3)$$

$$2Sb + 2O_2 \rightarrow Sb_2O_4 \qquad (S4)$$

Finally, the weight of the Sb@C composite samples retained stably at temperatures above 600 ºC. XRD patterns of the oxidation products of the Sb@C composite after the heating process and holding at 400 ºC and 700 ºC in air for 1 h are presented in **Fig. S1**c-d, respectively.

The weight percentage of Sb present in the Sb@C composite was calculated as follows.

$$Sb\ wt\% = \frac{2 \times weight\ (\%)_{at\ 700^oC}}{M_{Sb_2O_4}} \times M_{Sb}$$

where M_{Sb} and $M_{Sb_2O_4}$ are the molecular weights of Sb and Sb_2O_4, respectively, and the weight (%) at 700 ºC is the assumed weight of Sb_2O_4.

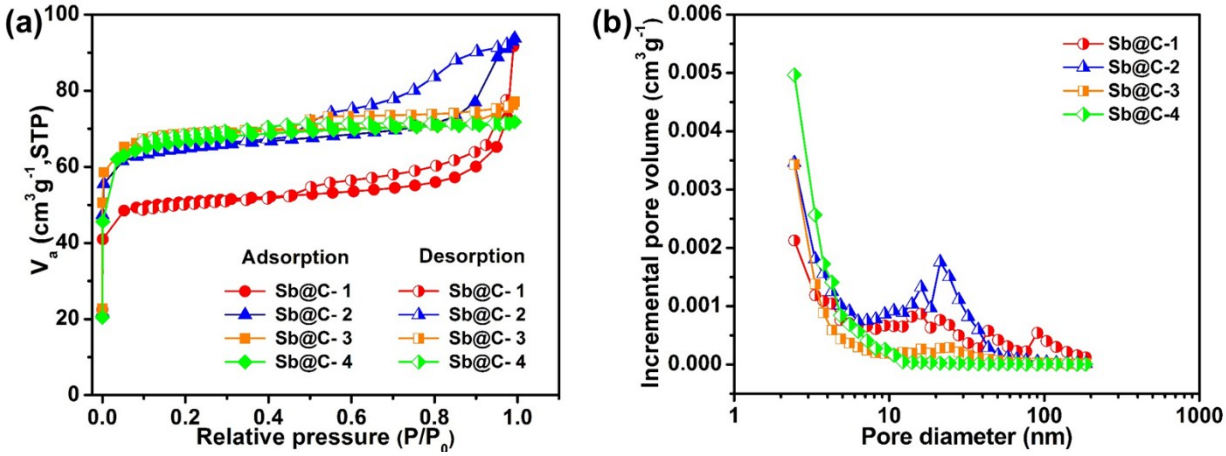

Fig. S2*: (a) Nitrogen adsorption-desorption isotherms and (b) cumulative pore volume of Sb@C-1, Sb@C-2, Sb@C-3, and Sb@C-4.*

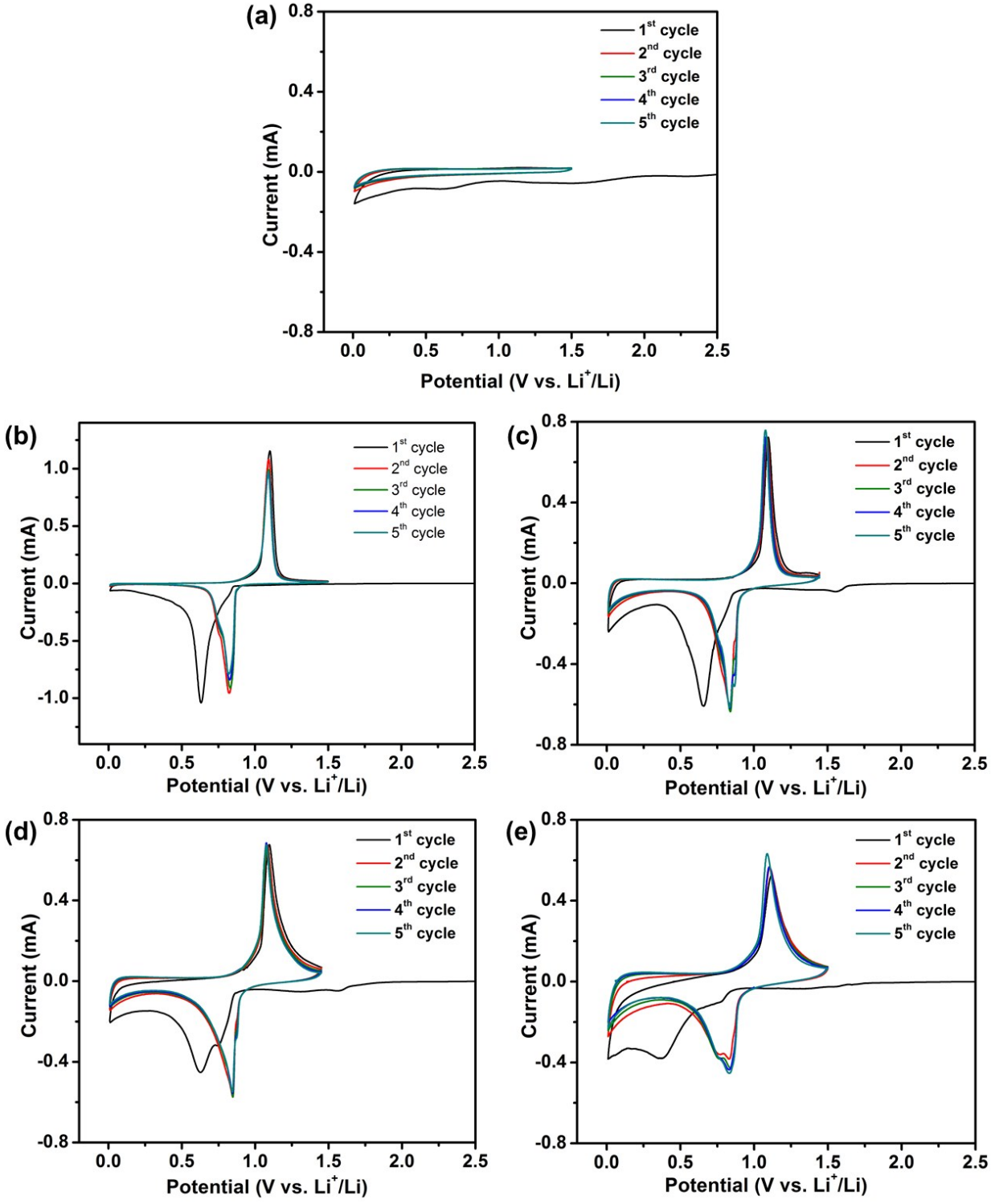

Fig. S3*: Cyclic voltammogram of electrodes: (a) pyrolytic carbon, (b) commercial Sb, (c) Sb@C-1, (d) Sb@C-2, and (e) Sb@C-4.*

As shown in **Fig. S3**a, at the first cathodic scan, the pyrolytic carbon electrode exhibits three peaks at 1.48 V, 0.59 V, and 0.01 vs. Li^+/Li. However, in the subsequent cycles two peaks at 1.48 and 0.59 V disappear completely, implying the irreversible formation of SEI layer on the surface of the electrode for the first cycle. In the 2^{nd} cycle onwards, only the sharp peak at 0.01 V corresponding to lithium intercalation into the carbon matrix remains. This is also verified by absence of the lithiation peak of carbon in the CV plots of the commercial Sb electrode, which does not contain any carbon material, as shown in **Fig. S3**b.

In comparison with the CV plots of the pyrolytic carbon (**Fig. S3**a) and the commercial Sb (**Fig. S3**b), all the CV plots of Sb@C composite electrodes (**Fig. S3**c-e) present the feature oxidation and reduction peaks of both Sb and carbon materials. This indicates similar electrochemical behaviors of these composite electrodes.

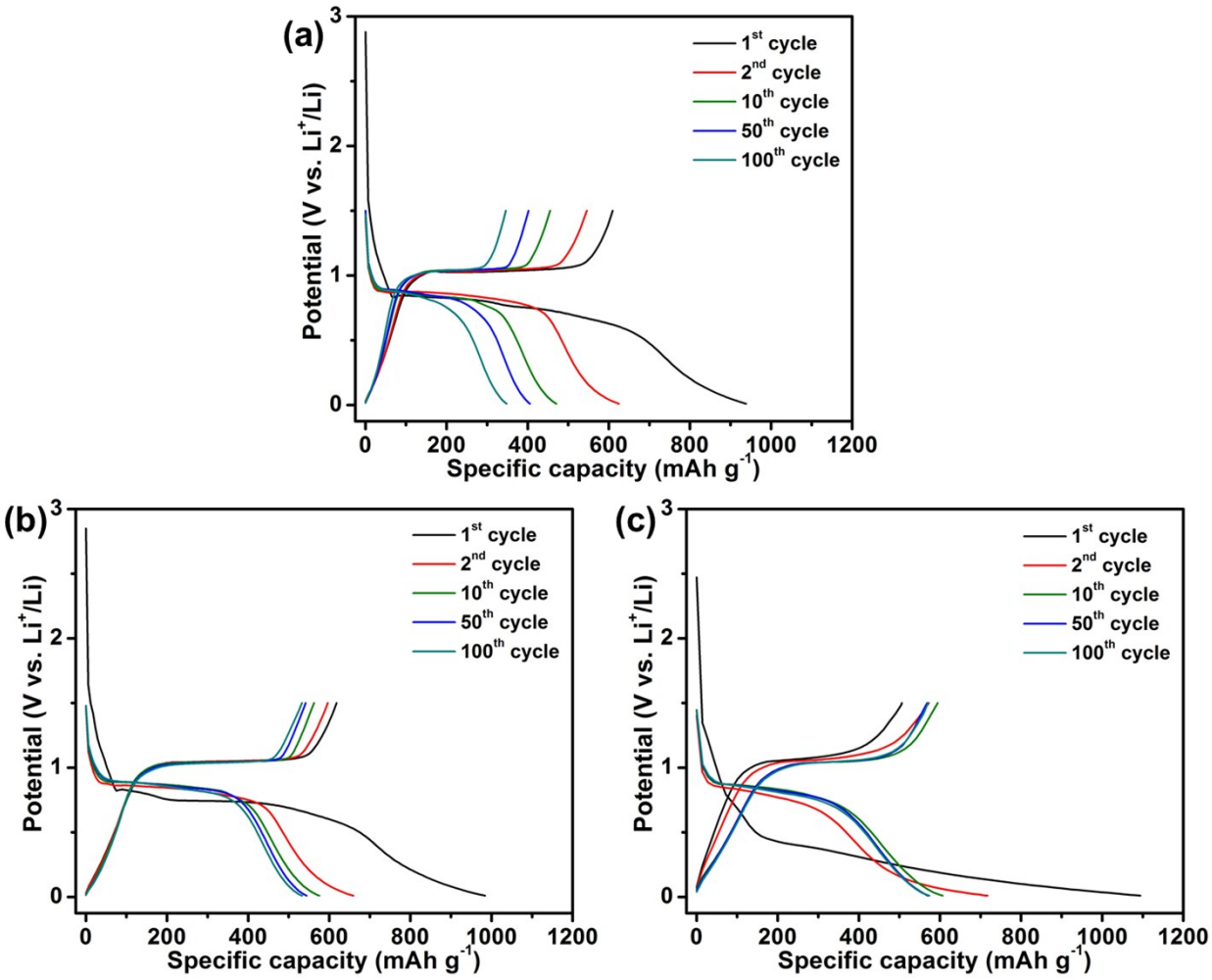

Fig. S4*: Discharge-charge potential profiles of (a) Sb@C-1 and (b) Sb@C-2, and (c) Sb@C-4 electrodes.*

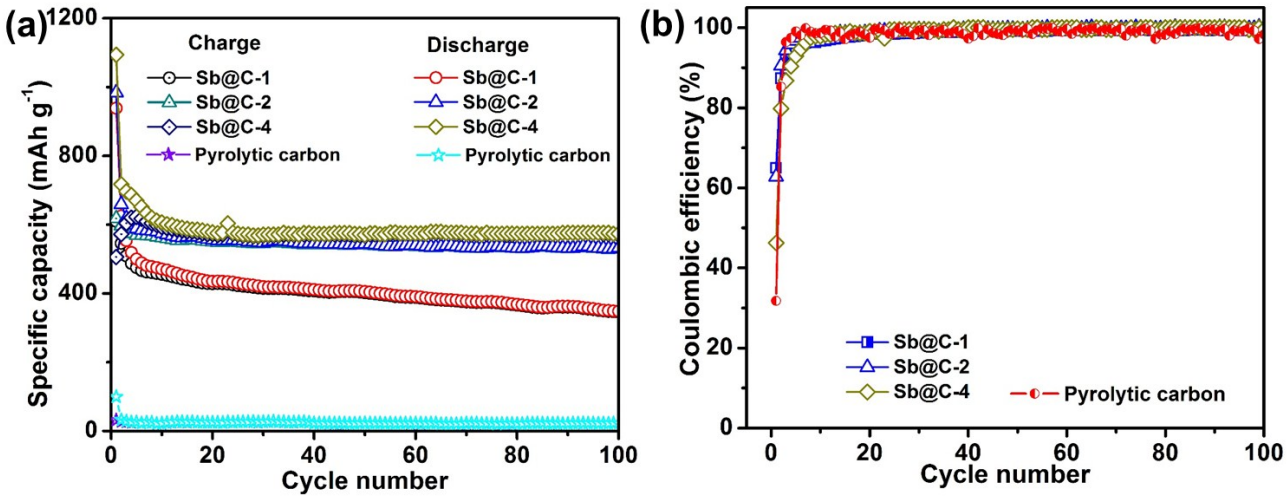

Fig. S5*: (a) Cyclability and (b) coulombic efficiency of Sb@C-1, Sb@C-2, Sb@C-4, and pyrolytic carbon electrodes at a rate of 0.1 C.*

In this study, in order to investigate the contribution of pure carbon derived from citric acid, we synthesized pyrolytic carbon with carbonized citric acid for 1 h in argon gas and then prepared the pyrolytic carbon electrode via a process that is analogous to that of the Sb@C composite electrodes. As shown in **Fig. S5**, the capacity contribution of pyrolytic carbon is almost insignificant. The pyrolytic carbon exhibits a low specific capacity of about 25 mAh g^{-1}. This value is negligible compared with the specific capacity of the Sb@C composite electrode.

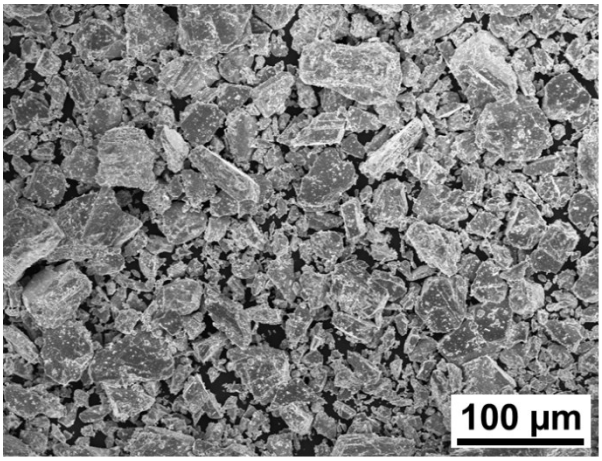

Fig. S6*: SEM image of commercial Sb powder.*

References

[1] T. Ramireddy, M. M. Rahman, T. Xing, Y. Chen and A. M. Glushenkov, *J. Mater. Chem. A*, 2014, **2**, 4282-4291.

[2] Y. Cheng, Z. Yi, C. Wang, L. Wang, Y. Wu and L. Wang, *Chem. Asian J.*, 2016, **11**, 2173-2180.

[3] X. Liu, Y. Tian, X. Cao, X. Li, Z. Le, D. Zhang, X. Li, P. Nie and H. Li, *ACS Appl. Mater. Interfaces*, 2018, **1**, 6381-6387.

[4] L. Fan, J. Zhang, J. Cui, Y. Zhu, J. Liang, L. Wang and Y. Qian, *J. Mater. Chem. A*, 2015, **3**, 3276-3280.

[5] Y. Wu, Q. Pan, F. Zheng, X. Ou, C. Yang, X. Xiong, M. Liu, D. Hu and C. Huang, *J. Alloys Compd.*, 2018, **744**, 481-486.

[6] Z. Yi, Q. Han, P. Zan, Y. Wu, Y. Cheng and L. Wang, *J. Power Sources*, 2016, **331**, 16-21.

[7] H. Lv, S. Qiu, G. Lu, Y. Fu, X. Li, C. Hu and J. Liu, *Electrochim. Acta*, 2015, **151**, 214-221.

[8] Y. NuLi, J. Yang and M. Jiang, *Materials Lett.*, 2008, **62,** 2092-2095.

[9] Q. Yang, J. Zhou, G. Zhang, C. Guo, M. Li, Y. Zhu and Y. Qian, *J. Mater. Chem. A*, 2017, **5**, 12144-12148.

[10] J. Liu, L. Yu, C. Wu, Y. Wen, K. Yin, F.-K. Chiang, R. Hu, J. Liu, L. Sun, L. Gu, J. Maier, Y. Yu and M. Zhu, *Nano Lett.*, 2017, **17**, 2034-2042.